energies

MDPI

Article

Optimization Strategy for Low-Carbon Economy of Integrated Energy System Considering Carbon Capture-Two Stage Power-to-Gas Hydrogen Coupling

Kangjie He [1], Linjun Zeng [2,*], Jun Yang [1], Yongguo Gong [2], Zhenhua Zhang [2] and Kun Chen [2]

[1] School of Electrical and Information Engineering, Changsha University of Science and Technology, Changsha 410000, China; yhoppp233@163.com (K.H.); 15521423189@163.com (J.Y.)
[2] School of Energy and Power Engineering, Changsha University of Science and Technology, Changsha 410000, China; a1147585967@outlook.com (Y.G.); 15676211816@163.com (Z.Z.); 23106011250@stu.csust.edu.cn (K.C.)
* Correspondence: zenglj@hnu.edu.cn

Abstract: To further optimize the low-carbon economy of the integrated energy system (IES), this paper establishes a two-stage P2G hydrogen-coupled electricity–heat–hydrogen–gas IES with carbon capture (CCS). First, this paper refines the two stages of P2G and introduces a hydrogen fuel cell (HFC) with a hydrogen storage device to fully utilize the hydrogen energy in the first stage of power-to-gas (P2G). Then, the ladder carbon trading mechanism is considered and CCS is introduced to further reduce the system's carbon emissions while coupling with P2G. Finally, the adjustable thermoelectric ratio characteristics of the combined heat and power unit (CHP) and HFC are considered to improve the energy utilization efficiency of the system and to reduce the system operating costs. This paper set up arithmetic examples to analyze from several perspectives, and the results show that the introduction of CCS can reduce carbon emissions by 41.83%. In the CCS-containing case, refining the P2G two-stage and coupling it with HFC and hydrogen storage can lead to a 30% reduction in carbon emissions and a 61% reduction in wind abandonment costs; consideration of CHP and HFC adjustable thermoelectric ratios can result in a 16% reduction in purchased energy costs.

Keywords: carbon capture; two-stage P2G; HFC; adjustable thermoelectric ratio; low carbon economics

Citation: He, K.; Zeng, L.; Yang, J.; Gong, Y.; Zhang, Z.; Chen, K. Optimization Strategy for Low-Carbon Economy of Integrated Energy System Considering Carbon Capture-Two Stage Power-to-Gas Hydrogen Coupling. *Energies* **2024**, *17*, 3205. https://doi.org/10.3390/en17133205

Academic Editor: Alberto Pettinau

Received: 13 May 2024
Revised: 16 June 2024
Accepted: 17 June 2024
Published: 29 June 2024

1. Introduction

The China's "14th Five-Year Plan" put forward the strategic goal of "carbon peak, carbon neutral" [1], and green low-carbon construction has become an important task for the present and the future [2–4]. IES can couple and coordinate multiple energy sources such as electricity, heat, gas, and hydrogen, and fully consider the complementary characteristics of each energy source. This property of IES is important for enhancing energy efficiency, reducing the impact of energy on the environment and thus promoting decarbonization [5,6].

The current studies on optimizing the low carbon economics of IES are mainly divided into the introduction of P2G, the introduction of CCS, the consideration of CHP or HFC with adjustable heat-to-power ratios, and the consideration of the ladder carbon trading mechanism [7]. The ladder carbon trading mechanism can effectively promote the low-carbon operation of IES through the price mechanism. Ref. [8] indicated that the ladder carbon trading mechanism can effectively reduce IES carbon emissions. Ref. [9] proposed a multi-timescale optimal scheduling method for integrated energy system under the ladder carbon trading mechanism, which reduces the system operation costs and system's carbon emissions. Ref. [10] constructed a combined electricity–gas–heat storage structure based on an energy conversion and storage device, introduced a ladder carbon trading mechanism to establish a hierarchical calculation model, and found that although the laddered carbon

trading increased the system cost, the carbon emissions were greatly reduced. From the above literature, it can be seen that the carbon emissions of IES can be reduced to a certain extent by considering the ladder carbon trading mechanism, so this paper will consider the ladder carbon trading mechanism when carrying out the mathematical model construction. However, this study also considers the coupling of hydrogen energy through the introduction and refinement of the two stages of P2G, as well as the introduction of CCS and HFC, and hydrogen storage to further improve the low-carbon economy of IES.

Some other ways of improving the low-carbon economy of IES include introducing CCS and P2G into the system. P2G, as a device that uses electricity to convert CO_2 to methane, is also relevant for reducing carbon emissions, while CCS can capture and sequester CO_2 efficiently, and the consideration of coupling CCS and P2G can further contribute to the low-carbon and economic operation of IES. Ref. [11] proposed a new low-carbon planning model for integrated electricity–gas–heat energy systems that considered the coupling of CCS and P2G, and the results showed that this strategy reduced system's carbon emissions and wind abandonment costs. Ref. [12] proposed a distributed robust low-carbon optimization strategy for an integrated energy system with CCS, utilization and sequestration-P2G synergistic operation, modeled the P2G process in a refined way, and investigated the multifaceted benefits of hydrogen energy, which improved the wind-scape consumption rate and economy of IES and reduced the carbon emissions of the system. Ref. [13] proposed a low-carbon optimal scheduling strategy for an integrated energy system that takes into account the integrated demand response and the joint operation of carbon capture-electricity-to-gas at multiple time scales, which makes full use of the source and load resources to participate in the regulation and realizes the system's low-carbon, economic, and stable operation. Ref. [14] proposed a low-carbon economic operation strategy that combines the characteristics of flexible loads on the demand side and operates in conjunction with CHP, CCS and P2G, which reduced the system peaking pressure, drastically lowered the system operation costs, and realized the synergy between economy and low carbon. Ref. [15] established a two-stage robust optimization model for the electricity–heat–gas–cooling IES by considering the characteristics of the cogeneration model with P2G and CCS, and constructed a cogeneration model considering P2G and CCS, which strengthened the ability to absorb new energy sources, reduced the carbon emissions, and lowered the total system cost. However, the above studies can improve their models to further optimize the results. For example, ref. [12] could also consider refining the two phases of P2G and introducing HFC and hydrogen storage coupled with it to further reduce the carbon emissions and improve the system economics. Ref. [14] could also consider making full use of hydrogen energy by introducing HFC equipment and investigating the ladder carbon trading mechanism to further improve the low-carbon economics of IES.

Considering the adjustable characteristics of the system's thermoelectric ratio can improve the efficiency of energy utilization, thus increasing the economy of the system in the same situation. Ref. [16] constructed an optimal scheduling model of a township's integrated energy system based on an adjustable heat and power ratio model and proposed a scheme for adjusting the heat and power ratio. The optimization results showed that the economic cost of considering the adjustable heat and power ratio was lower than not considering those factors, and the utilization rate of clean energy was also higher. Ref. [17] proposed an optimal scheduling model for an IES considering a renewable enhanced geothermal system and an adjustable heat-to-power ratio, which improved the system economics and wind power consumption rate, and reduced carbon emissions; however, the study did not consider that the introduction of CCS and the ladder carbon trading mechanism could further improve the low-carbon economic operation of the system. Ref. [18] constructed a low-carbon economic optimization dispatch model for IES from the participation of IES to the ladder carbon trading market, refinement of the two-stage operation process of P2G, and consideration of the adjustable characteristics of CHP and HFC heat-to-power ratios; however, the study did not consider that the introduction of

CCS could further reduce the carbon emissions of the system, as well as reduce the total operating costs of the system. Table 1 lists the references and the contributions to this paper. In Table 1, "√" indicates that the item was considered in the literature, while "×" indicates that the item was not considered.

Table 1. Overview of reference contributions.

Reference	Ladder Carbon Trading Mechanism	CCS	P2G	HFC	CHP	Adjustable Thermoelectric Ratio
[8]	√	×	×	×	×	×
[9]	√	×	×	×	√	×
[10]	√	×	√	×	×	×
[11]	√	√	√	×	×	×
[12]	√	√	√	√	√	×
[13]	×	√	√	×	×	×
[14]	×	√	√	×	√	×
[15]	×	√	√	×	√	×
[16]	×	×	×	×	√	√
[17]	×	×	√	×	√	√
[18]	√	×	√	√	√	√
this article	√	√	√	√	√	√

All the schemes proposed in the above studies can effectively improve the low-carbon economics of IES, but few studies have considered coupling CCS with P2G after refining the two stages and considering the adjustable thermoelectric ratio characteristics of CHP and HFC to further improve the low-carbon economics of IES. To this end, this paper will establish an integrated energy system considering a two-stage P2G hydrogen-coupled CCS-containing system, with the introduction of a ladder carbon trading mechanism, and the consideration of the adjustable heat-to-power ratio characteristics of CHP and HFC. Then, examples are set up to study the effect of the carbon capture system on the improvement of IES economy and low carbon, as well as the effect of the ladder carbon trading mechanism, the refinement of the two-stage P2G and CHP, and the adjustable heat-to-electricity ratio characteristics of HFC on the improvement of the system efficiency for IES with CCS. This paper contributes the following:

1. The IES of CCS two-stage P2G hydrogen coupling is constructed, coupling CCS, two-stage P2G, and HFC, and at the same time, considering the ladder carbon trading mechanism and the adjustable heat-to-electricity ratio characteristics of CHP and HFC, which fully reduce the carbon emissions of the system and ensure the economic operation of the system;
2. Refine the two stages of P2G and couple it with HFC and hydrogen storage to make full use of the H_2 generated in the first stage of P2G, share part of the load of CHP and GB while reducing the loss of energy gradient, reduce the carbon emissions of the system, and optimize the IES economy;
3. Considering the adjustable thermoelectric ratio characteristics of CHP and HFC to further balance the supply and demand of electricity and heat in the system, reduce energy waste, and thus optimize the IES economics;
4. By introducing CCS and simultaneously considering the ladder carbon trading mechanism, refining the two-stage P2G, CHP and HFC adjustable thermoelectric ratio characteristics, i.e., simultaneously introducing a variety of methods to optimize the low-carbon economics of the IES, with the various methods complementing each other, thus greatly improving the low-carbon economics of the IES.

The remainder of this paper will outline the specific modeling of IES and the setting of constraints and objective functions, and finally set up the arithmetic examples from three aspects to analyze and draw conclusions. The second part provides the modeling of the two-stage P2G hydrogen-coupled integrated energy system with CCS, the third part is the

operational modeling of two-stage P2G hydrogen-coupled IES with CCS, the fourth part provides the analysis of the arithmetic example, and the last part is the conclusion.

The flow of this paper is shown in the following flowchart (Figure 1):

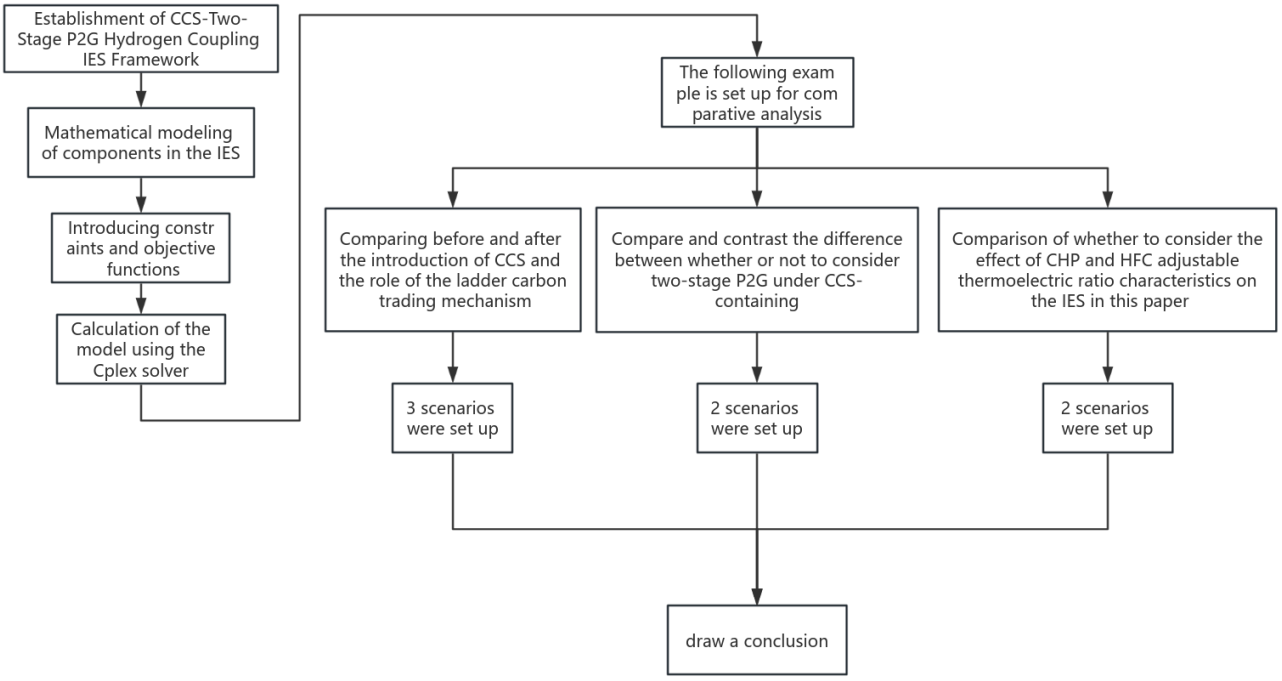

Figure 1. The methodology used in this paper.

2. Modeling of Two-Stage P2G Hydrogen-Coupled Integrated Energy System with CCS

This paper proposed an integrated energy system whose energy inputs include externally purchased electricity, externally purchased gas, and wind power, whose energy storage devices include electricity, gas, heat, and hydrogen storage devices, and whose energy conversion devices include gas boiler (GB), combined heat and power (CHP), power-to-gas (P2G) and hydrogen fuel cell (HFC). The energy sources were coupled with each other through energy conversion equipment, which could be flexibly converted and dispatched, thus making full use of all types of energy and maximizing the economic benefits. Meanwhile, this paper further reduced carbon emissions by introducing a carbon capture (CCS) device into the system while considering the ladder carbon trading mechanism, the adjustable thermoelectric ratio characteristics of CHP and HFC, and two-stage utilization of P2G. The IES framework of this paper is shown in Figure 2.

As can be seen from Figure 1, the energy inputs to the IES built in this paper include wind, electricity, and natural gas, where electricity is partly supplied to the electric load and partly to the EL for hydrogen production. Natural gas is partly supplied to the gas load and partly supplied to GB for heat production and CHP for electricity and heat production. In addition, the system also incorporates electric, gas, and thermal energy storage devices, and introduces MR and CCS to jointly convert the hydrogen produced by EL into natural gas for CHP, and HFC to make full use of the hydrogen produced by EL to produce electricity and heat. Most of the CO_2 produced by this system will be absorbed by the CCS and fully utilized.

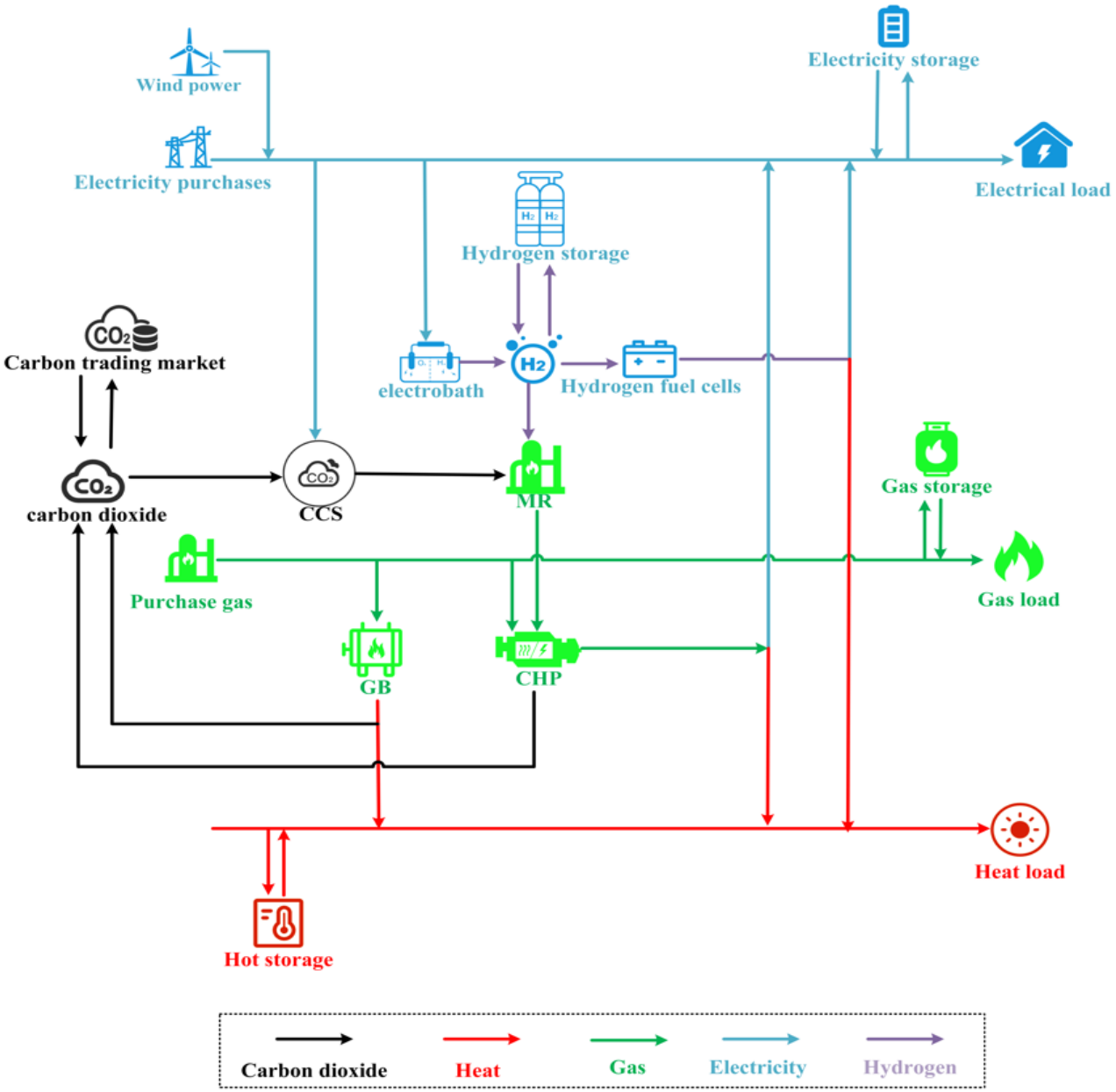

Figure 2. Two-stage P2G hydrogen-coupled IES with CCS.

2.1. Two-Stage P2G Hydrogen Coupling Modeling

P2G is a device that consumes electricity to convert CO_2 into methane (CH_4) and consists of two parts: an electrolysis cell (EL) and a methane reactor (MR). The operation of P2G can be divided into two stages: the first stage is the generation of hydrogen using EL, and the second stage is the generation of CH_4, the main component of natural gas, which can be used to supply gas loads, GB, and CHP, from the hydrogen and CO_2 generated in the first stage through MR. As electricity is first converted into hydrogen and then into natural gas for use by the unit, after two energy transformations, there is bound to be a gradual loss of energy. For this reason, in this paper, P2G is refined into two stages, the hydrogen produced in the first stage is fully utilized, and a portion of the hydrogen is directly converted into electrical and thermal energy by introducing HFC. The efficiency of this process is much higher than the efficiency of directly converting electrical energy into natural gas and then supplying it to the unit to be burned to produce electrical and thermal energy. Therefore, it is of great importance to refine the P2G two-stage operation process. Meanwhile, CCS is added in this paper, which can be coupled with P2G to make the P2G

conversion process more efficient. The above energy conversion process is modeled for each device as follows:

(1) EL equipment

$$\begin{cases} P_{el\_H_2}(t) = \eta_{el} P_{e\_el}(t) \\ P_{e\_el}^{\min} \le P_{e\_el}(t) \le P_{e\_el}^{\max} \\ \Delta P_{e\_el}^{\min} \le P_{e\_el}(t+1) - P_{e\_el}(t) \le \Delta P_{e\_el}^{\max} \end{cases} \tag{1}$$

where $P_{el\_H_2}(t)$ and $P_{e\_el}(t)$ are the hydrogen energy output from the EL and the electrical energy input to the EL, respectively. $P_{e\_el}^{\max}$, $P_{e\_el}^{\min}$ and $\Delta P_{e\_el}^{\max}$, $\Delta P_{e\_el}^{\min}$ are the electrical energy input to EL and the upper and lower limits of the EL climb, respectively. η_{EL} is the energy conversion efficiency of EL.

(2) MR equipment

$$\begin{cases} P_{mr\_g}(t) = \eta_{mr} P_{H_2\_mr}(t) \\ P_{H_2\_mr}^{\min} \le P_{H_2\_mr}(t) \le P_{H_2\_mr}^{\max} \\ \Delta P_{H_2\_mr}^{\min} \le P_{H_2\_mr}(t+1) - P_{H_2\_mr}(t) \le \Delta P_{H_2\_mr}^{\max} \end{cases} \tag{2}$$

where $P_{H_2\_mr}(t)$ is the hydrogen energy input to the MR at time period t; η_{mr} is the efficiency of MR; $P_{mr\_g}(t)$ is the gas power output from MR at time t and $P_{H_2\_mr}^{\max}$, $P_{H_2\_mr}^{\min}$ and $\Delta P_{H_2\_mr}^{\max}$, $\Delta P_{H_2\_mr}^{\min}$ are the hydrogen energy input to the MR and the upper and lower limits of the climb of the MR.

(3) HFC equipment

$$\begin{cases} P_{\text{hfc\_e}}(t) = \eta_{\text{hfc}}^{e} P_{H_2\_\text{hfc}}(t) \\ P_{\text{hfc\_h}}(t) = \eta_{\text{hfc}}^{h} P_{H_2\_\text{hfc}}(t) \\ P_{H_2\_\text{hfc}}^{\min} \le P_{H_2\_\text{hfc}}(t) \le P_{H_2\_\text{hfc}}^{\max} \\ \Delta P_{H_2\_\text{hfc}}^{\min} \le P_{H_2\_\text{hfc}}(t+1) - P_{H_2\_\text{hfc}}(t) \le \Delta P_{H_2\_\text{hfc}}^{\max} \\ k_{\text{hfc}}^{\min} \le P_{\text{hfc\_}h}(t) / P_{\text{hfc\_}e}(t) \le k_{\text{hfc}}^{\max} \end{cases} \tag{3}$$

where $P_{\text{hfc\_e}}(t)$ is the electrical energy output from the HFC at time period t; $P_{\text{hfc\_h}}(t)$ is the thermal energy output from the HFC in time period t; $P_{H_2\_\text{hfc}}(t)$ is the hydrogen energy input to the HFC at time t; $P_{H_2\_\text{hfc}}^{\max}$ and $P_{H_2\_\text{hfc}}^{\min}$ are the upper and lower limits of the hydrogen energy input to the HFC; $\Delta P_{H_2\_\text{hfc}}^{\max}$ and $\Delta P_{H_2\_\text{hfc}}^{\min}$ are the upper and lower limits of HFC creep; $\eta_{\text{hfc}}^{\text{e}}$ is the efficiency of HFC conversion to electrical energy; $\eta_{\text{hfc}}^{\text{h}}$ is the efficiency of HFC conversion to heat and $k_{\text{hfc}}^{\max}$ and k_{hfc}^{min} are the upper and lower thermoelectric ratio limits for HFC, respectively.

2.2. CCS Model

CCS consists of carbon capture and carbon sequestration. Part of the captured CO_2 is fed into the P2G equipment through pipelines for recycling, and the other part is sequestered through a CO_2 compressor.

(1) The CCS consumes part of the electrical energy and captures and stores CO_2 from the system and uses the captured and stored CO_2 in the second stage of P2G for the production of CH_4 to supply the gas load and GB, which is modeled in Equation (4), as follows:

$$\begin{cases} P_{CCS}(t) = P_{CCS\_f}(t) + P_{CCS\_O}(t) \\ P_{CCS\_O}(t) = \varepsilon_{CCS} m_{CCS\_CO2}(t) \\ m_{CCS\_CO2}(t) = \omega_{CCS}(m_{GB\_CO2}(t) + m_{CHP\_CO2}(t)) \\ m_{CCS\_CO2}(t) = m_{MR\_CO2}(t) + m_{F\_CO2}(t) \end{cases} \tag{4}$$

where $P_{CCS}(t)$ is the total energy consumption of the CCS system at moment t; $P_{CCS\_f}(t)$ and $P_{CCS\_O}(t)$ are the fixed and operational energy consumption of the CCS system at

moment t and $m_{CCS\_CO2}(t)$ is the amount of CO_2 captured by the CCS at time t. $m_{GB\_CO2}(t)$ and $m_{CHP\_CO2}(t)$ are the amount of CO_2 produced by the GB and CHP units at the moment t, respectively. $m_{MR\_CO2}(t)$ is the amount of CO_2 consumed by methanation at moment t. $m_{F\_CO2}(t)$ is the amount of CO_2 sequestered at time t. ε_{CCS} is the power consumption per unit of CO_2 captured by CCS, which is taken as 0.1. ω_{CCS} is the carbon capture rate of CCS, which is taken as 0.58.

(2) The CCS operating power constraints and climbing power constraints are shown in the following Equation (5).

$$\begin{cases} P_{CCS}^{\min} \le P_{CCS}(t) \le P_{CCS}^{\max} \\ P_{CCS}^{\text{down}} \le P_{CCS}(t) - P_{CCS}(t-1) \le P_{CCS}^{\text{up}} \end{cases} \tag{5}$$

where $P_{CCS}^{\max}$, $P_{CCS}^{\min}$ and P_{CCS}^{up}, P_{CCS}^{down} are the upper and lower limits of the CCS electric power and the CCS power creep rate, respectively.

2.3. Adjustable Thermoelectric Ratio CHP Modeling

CHP is a device that consumes natural gas to generate electricity and heat at the same time, which generates electricity to supply electric loads and IES internal electric equipment, and heat to supply heat loads, and the CHP's thermoelectricity ratio is defined as the ratio of the heat supply power to the electricity supply power. The CHP with adjustable thermoelectric ratio can adjust its own thermoelectric output according to the electric heat load in a period of time, which can improve the efficiency of energy utilization. The adjustable thermoelectric ratio CHP operating model is shown in Equation (6).

$$\begin{cases} P_{chp\_e}(t) = \eta_{chp}^{e} P_{g\_chp}(t) \\ P_{chp\_h}(t) = \eta_{chp}^{h} P_{g\_chp}(t) \\ P_{g\_chp}^{\min} \le P_{g\_chp}(t) \le P_{g\_chp}^{\max} \\ \Delta P_{g\_chp}^{\min} \le P_{g\_chp}(t+1) - P_{g\_chp}(t) \le \Delta P_{g\_chp}^{\max} \\ k_{chp}^{\min} \le P_{chp\_h}(t) / P_{chp\_e}(t) \le k_{chp}^{\max} \end{cases} \tag{6}$$

where $P_{\text{chp\_}e}(t)$ is the electrical energy output from the CHP at time period t; $P_{g\_chp}(t)$ is the natural gas power input to the CHP at time t; $P_{\text{chp\_}h}(t)$ is the thermal energy output from CHP at time t; η_{chp}^{e} is the efficiency of CHP conversion to electrical energy; η_{chp}^{h} is the efficiency of conversion of CHP to heat; $P_{g\_chp}^{\max}$ and $P_{g\_chp}^{\min}$ are the upper and lower limits of the gas power input to the CHP; $\Delta P_{g\_chp}^{\max}$ and $\Delta P_{g\_chp}^{\min}$ are the upper and lower limits of the CHP climb and $k_{chp}^{\max}$ and $k_{chp}^{\min}$ are the upper and lower thermoelectric ratio limits for CHP, respectively.

2.4. Ladder Carbon Trading Mechanism

(1) Carbon emission allowances [19]

$$\begin{cases} E_{IES} = E_{e\_buy} + E_{CHP} + E_{GB} \\ E_{e\_buy} = \tau_e \sum_{t=1}^{T} P_{e\_buy}(t) \\ E_{CHP} = \tau_g \sum_{t=1}^{T} \left(\mu_h^e P_{chp\_e}(t) + P_{chp\_h}(t) \right) \\ E_{GB} = \tau_g \sum_{t=1}^{T} P_{gb\_h}(t) \end{cases} \tag{7}$$

where E_{IES} represents the total carbon credits of IES; $E_{\text{e\_}buy}$, E_{CHP} and E_{GB} are carbon credit allowances for external power purchase, CHP, and GB, respectively; $P_{\text{e\_}buy}(t)$ is the amount of power purchased by IES in time period t; $P_{\text{gb\_h}}(t)$ is the thermal energy output from GB at time period t; $\mu_{\text{h}}^{\text{e}}$ is the electrical-to-thermal conversion factor τ_{e} and τ_{g} are

the carbon emission allowance coefficients per unit for external thermal power units and natural gas-fired units, respectively.

(2) Actual carbon emissions

A part of CO_2 will be absorbed in the process of hydrogen to natural gas conversion of the P2G two-stage MR equipment in the system, and the carbon emissions reduced by CCS should also be considered, so the actual carbon emission model is shown in (8), as follows:

$$\begin{cases} E_{IES,a} = E_{e,buy,a} + E_{GB,a} + E_{CHP,a} - E_{MR,a} - E_{CCS\_F,a} \\ E_{e,buy,a} = \varepsilon_e \sum_{t=1}^{T} P_{e\_buy}(t) \\ E_{CHP,a} = \varepsilon_g \sum_{t=1}^{T} (\mu_h^e P_{chp\_e}(t) + P_{chp\_h}(t)) \\ E_{GB,a} = \varepsilon_g \sum_{t=1}^{T} P_{gb\_h}(t) \\ E_{MR,a} = \varpi_{mr} \sum_{t=1}^{T} P_{mr\_g}(t) \\ E_{CCS\_F,a} = \sum_{t}^{T} m_{CCS\_F}(t) \end{cases} \tag{8}$$

where $E_{IES,a}$ is the total IES carbon emissions; $E_{e,buy,a}$, $E_{CHP,a}$, $E_{GB,a}$ are the carbon emissions from the upstream power purchase, CHP, and GB operation processes, respectively; $E_{MR,a}$ and $E_{CCS\_F,a}$ are the actual carbon emissions reduced by MR and CCS, respectively; ε_e is the carbon emission factor for thermal power purchased from the grid, which is taken as 1.08; ε_g is the carbon emission factor of natural gas energy supply for GB and CHP, which is taken as 0.234 and ϖ_{mr} is a parameter for CO_2 absorption in the hydrogen to natural gas process of MR equipment.

(3) Carbon trading costs

From the carbon emission quotas, the actual carbon emissions can be derived from the participation in the carbon trading market carbon emission trading amount, that is, the net carbon emissions E, as shown in Equation (9). The specific algorithm for carbon trading costs is shown in Equation (10), as follows:

$$E = E_{IES,a} - E_{IES} \tag{9}$$

$$C_{CO2} = \begin{cases} \lambda E & E \le d \\ \lambda(1+\alpha)(E-d) + \lambda d & d \le E \le 2d \\ \lambda(1+2\alpha)(E-d) + \lambda(2+\alpha)d & 2d \le E \le 3d \\ \lambda(1+3\alpha)(E-d) + \lambda(3+3\alpha)d & 3d \le E \le 4d \\ \lambda(1+4\alpha)(E-d) + \lambda(4+6\alpha)d & E \ge 4d \end{cases} \tag{10}$$

In Equation (10), C_{CO2} is the cost of carbon trading; λ is the carbon trading base price; d is the length of the carbon emission interval and α is the price growth rate.

3. IES Operation Model

3.1. Objective Function

In this paper, the total cost of system operation is minimized as the objective function, and the IES optimization objective is to minimize the total cost C. The total operating costs include: purchased energy costs C_{buy}, the ladder carbon trading costs C_{CO2} and the wind abandonment costs C_{PG_cut}. The costing approach proposed above is shown below:

(1) Total cost objective function

$$C = \min(C_{buy} + C_{CO2} + C_{PG\_cut}) \tag{11}$$

(2) Cost of purchased energy

$$\begin{cases} C_{buy} = C_{buy\_e} + C_{buy\_g} \\ C_{buy\_e} = \sum_{t=1}^{T} \pi_{e\_t} P_{e\_buy}(t) \\ C_{buy\_g} = \sum_{t=1}^{T} \pi_{g\_t} P_{g\_buy}(t) \end{cases} \tag{12}$$

where C_{buy} is the total purchased energy cost; C_{buy_e} and C_{buy_g} are the cost of electricity and gas purchases; $P_{g\_buy}(t)$ is the volume of gas purchased in time period t and π_{e_t} and π_{g_t} are the electricity and gas prices in time period t, respectively.

(3) Carbon trading costs: as shown in Equation (10).

(4) Wind abandonment costs

$$C_{PG\_cut} = \delta_{DG} \sum_{t=1}^{T} P_{DG\_cut} \tag{13}$$

In Equation (13), δ_{DG} is the cost per unit of abandoned wind penalty and $P_{DG\_cut}(t)$ is the abandoned wind power at time period t.

3.2. Model Run Constraints

(1) CCS power constraint: as shown in Equation (5).

(2) EL, MR, HFC, CHP operating constraints: as shown in Equations (1), (2), (3) and (6).

(3) GB operational constraints as shown below:

$$\begin{cases} P_{gb\_h}(t) = \eta_{gb} P_{g\_gb}(t) \\ P_{g\_gb}^{\min} \le P_{g\_gb}(t) \le P_{g\_gb}^{\max} \\ \Delta P_{g\_gb}^{\min} \le P_{g\_gb}(t+1) - P_{g\_gb}(t) \le \Delta P_{g\_gb}^{\max} \end{cases} \tag{14}$$

where η_{gb} is the energy conversion efficiency of GB; $P_{g\_gb}(t)$ is the power input to GB at time t; $P_{g\_gb}^{\max}$ and $P_{g\_gb}^{\min}$ are the upper and lower input power limits of GB, respectively, and $\Delta P_{g\_gb}^{\max}$ and $\Delta P_{g\_gb}^{min}$ are the upper and lower limits of climb for GB, respectively.

(4) Energy storage operational constraints.

Ref. [20] shows that the models of each energy storage device in the IES are similar. So, in this paper, all the energy storage devices are modeled uniformly, as shown in Equation (16).

$$\begin{cases} 0 \le P_{ES,n}^{cha}(t) \le B_{ES,n}^{cha}(t) P_{ES,n}^{\max} \\ 0 \le P_{ES,n}^{dis}(t) \le B_{ES,n}^{dis}(t) P_{ES,n}^{\max} \\ P_{ES,n}(t) = P_{ES,n}^{cha}(t) \eta_{ES,n}^{cha} - P_{ES,n}^{dis}(t) / \eta_{ES,n}^{dis} \\ S_n(t) = S_n(t-1) + P_{ES,n}(t) / P_{ES,n}^{cap} \\ S_n(1) = S_n(T) \\ B_{ES,n}^{cha}(t) + B_{ES,n}^{dis}(t) = 1 \\ S_n^{\min} \le S_n(t) \le S_n^{\max} \end{cases} \tag{15}$$

where $P_{ES,n}^{\max}$ denotes the maximum power of the nth type of energy storage device for a particular charge and discharge; $B_{ES,n}^{cha}(t)$ and $B_{ES,n}^{dis}(t)$ are the binary variable used to represent the charging and discharging state of the nth energy storage device at time period t. The value at any moment can only be 0 or 1. Where the former indicates that it is in the energized state and the latter indicates that it is in the discharged state, and only one of the two state variables can take 1, this indicates that it is in that state. $P_{ES,n}(t)$ is the final output power of the nth energy storage device. $P_{ES,n}^{cha}(t)$ and $P_{ES,n}^{\text{dis}}(t)$ are the charging and discharging power of the nth energy storage device at time t, respectively. $\eta_{ES,n}^{cha}$ and $\eta_{ES,n}^{\text{dis}}$

are the charging and discharging efficiencies of the nth energy storage device, respectively. $S_n(t)$ is the capacity of the nth energy storage device at time t. $S_n^{\max}$ and $S_n^{\min}$ are the upper and lower limits of the capacity of the nth energy storage device, respectively. $P_{ES,n}^{cap}$ is the rated capacity of the nth energy storage device.

(5) Wind power output constraints as shown below:

$$0 \le P_{DG}(t) \le P_{DG}^{\max} \tag{16}$$

where $P_{DG}(t)$ is the wind power output at time period t and $P_{DG}^{\max}$ is the upper limit of wind power output.

(6) Electrical power balance constraints as shown below:

$$\begin{cases} P_{e\_buy}(t) = P_{e\_load}(t) + P_{CCS}(t) + P_{e\_el}(t) + P_{ES\_e}(t) \\ \qquad -P_{DG}(t) - P_{chp\_e}(t) - P_{hfc\_e}(t) \\ 0 \le P_{e\_buy}(t) \le P_{e\_buy}^{\max} \end{cases} \tag{17}$$

where $P_{e\_load}(t)$ is the electrical load at time t; $P_{ES\_e}(t)$ is the power input to the power storage device in time period t; $P_{e\_buy}^{\max}$ is the power purchase limit for each time period and $P_{CCS}(t)$ is the electric power consumed by the CCS at time t.

(7) Thermal power balance constraints

$$P_{\mathrm{hfc}\_h}(t) + P_{chp\_h}(t) + P_{gb\_\mathrm{h}}(t) = P_{h\_load}(t) + P_{ES\_h}(t) \tag{18}$$

where $P_{\mathrm{h}\_load}(t)$ is the heat load at time t. $P_{ES\_h}(t)$ is the power input to the thermal storage at time t.

(8) Gas power balance constraints as shown below:

$$\begin{cases} P_{g\_buy}(t) = P_{g\_load}(t) + P_{ES}^{g}(t) + P_{g\_chp}(t) \\ \qquad +P_{g\_gb}(t) - P_{mr\_g}(t) \\ 0 \le P_{g\_buy}(t) \le P_{g\_buy}^{\max} \end{cases} \tag{19}$$

where $P_{g\_load}(t)$ is the gas load at time period t; $P_{ES\_g}(t)$ is the power input to the natural gas storage at time t and $P_{g\_buy}^{\max}$ is the gas purchase limit for each time period.

(9) Hydrogen equilibrium constraints as shown below:

$$P_{el\_H_2}(t) = P_{H_2\_mr}(t) + P_{H_2\_hfc}(t) + P_{ES}^{H_2}(t) \tag{20}$$

where $P_{ES}^{H_2}(t)$ is the power input to the hydrogen storage at time t.

4. Example Analysis

To verify the effectiveness of the IES system containing carbon capture CCS proposed in this paper for the operation of a low-carbon economy, an arithmetic example is set up for verification. Let the scheduling period T = 24 h and each time slot Δt = 1 h. The results of the various load and turbine output predictions within the IES are shown in Figure 3. Since the focus of this paper is not to account for the impact of wind power uncertainty on IES, it is assumed that the wind power output is fixed at each time of the day, and the impact of load fluctuations is also not taken into account. In order to make the example results more accurate, the time-of-use tariffs and natural gas tariffs, the installed capacity and operating parameters of each device, and the installed capacity and parameters of each energy storage are taken from Ref. [18] (see Appendix A for specific parameters). The operating parameters of the CCS devices are shown in Table 2. Taking the carbon credit allowance per unit of electricity consumed by a coal-fired unit τ_e = 0.68 kg/(kW·h), the

carbon credit allowance per unit of natural gas consumed by natural gas-fired units is τ_g = 0.3672 kg/(kW·h) and the unit wind penalty cost is δ_{DG} = 0.2 yuan/(kW·h).

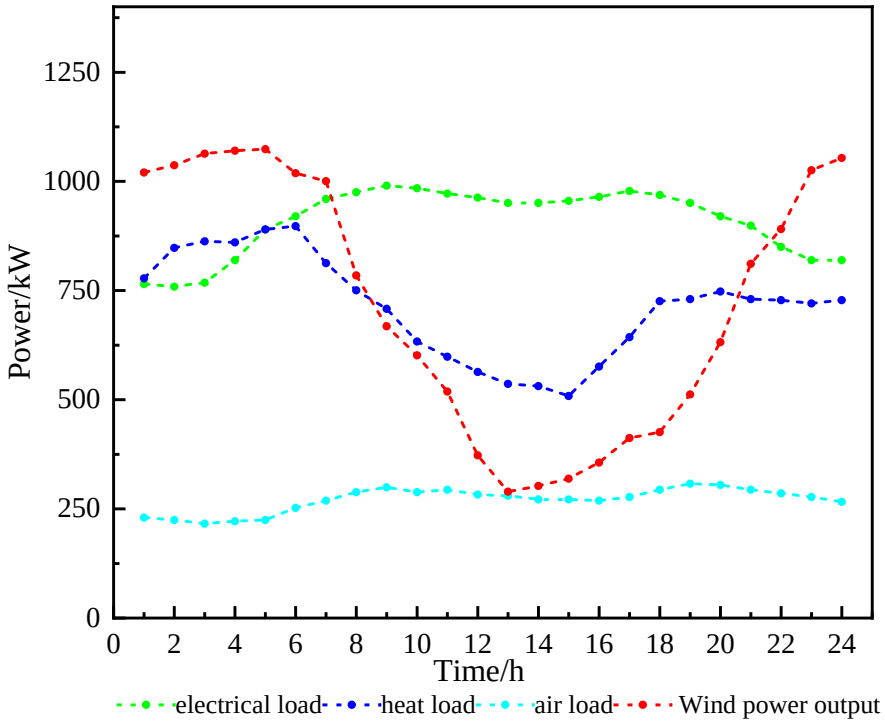

Figure 3. Prediction chart of each load and turbine output.

Table 2. CCS equipment operating parameters.

Parameter Type	Value
Capacity (kW)	1500
Electricity consumption for carbon capture (kW/kg)	0.1
Carbon capture rate	0.58
Climbing constraints	20%
Fixed energy consumption (kW)	10

The environment for all results in this example: Windows 11 @CPU AMD Ryzen™ 7 5800H; @GPU RTX3060. Programming tools used for this example: MATLAB R2022b and CPLEX solver IBM 12.10.0.

4.1. Analysis of CCS and Ladder Carbon Trading Mechanism

(1) CCS and ladder carbon trading mechanism benefit analysis

To verify the effectiveness of considering CCS on the system's carbon emissions as well as reducing the total costs of system operation and the benefits of ladder carbon trading proposed in this paper, this paper sets the length of each interval of the ladder carbon trading d = 500 kg, the price growth rate $\alpha = 0.25$, and the base value of the carbon trading CNY $\lambda = 0.25$/kg, and at the same time, the following three scenarios are established for comparative analysis.

Scenario 1: The traditional economic dispatch scenario without considering the ladder carbon trading mechanism and without introducing CCS.

Scenario 2: The low-carbon optimized dispatch scenario considering the ladder carbon trading mechanism but without introducing CCS.

Scenario 3: The optimized scheduling scenario for low carbon economy considering ladder carbon trading mechanism and introducing CCS.

Table 3 shows the results of comparing the benefits of each scenario in terms of five dimensions: carbon emissions, purchased energy costs, carbon trading costs, wind abandonment costs, and total costs. As can be seen from the table, the total carbon emissions of the system when CCS is introduced are much smaller than the total carbon emissions of the system when CCS is not taken into account, and due to the greatly reduced carbon emissions, the carbon trading cost is also greatly reduced, which ultimately leads to a significant reduction in the total operating costs of the system as well. Figure 4 illustrates a visual comparison of Scenario 1, Scenario 2, and Scenario 3.

Table 3. Comparison of CCS and ladder carbon trading mechanisms by scenario.

Optimization Results	Scenario 1	Scenario 2	Scenario 3
Carbon emissions/kg	4492.2042	4433.8803	2579.1788
Carbon trading costs/CNY	1123.0510	1904.4401	977.0894
Power purchase cost/CNY	0.0000	1.2814	160.6512
Purchased gas cost/CNY	6365.6013	6388.0239	6452.4744
Wind abandonment cost/CNY	65.3458	63.5862	56.7749
Total cost/CNY	7553.9982	8357.3316	7646.9899

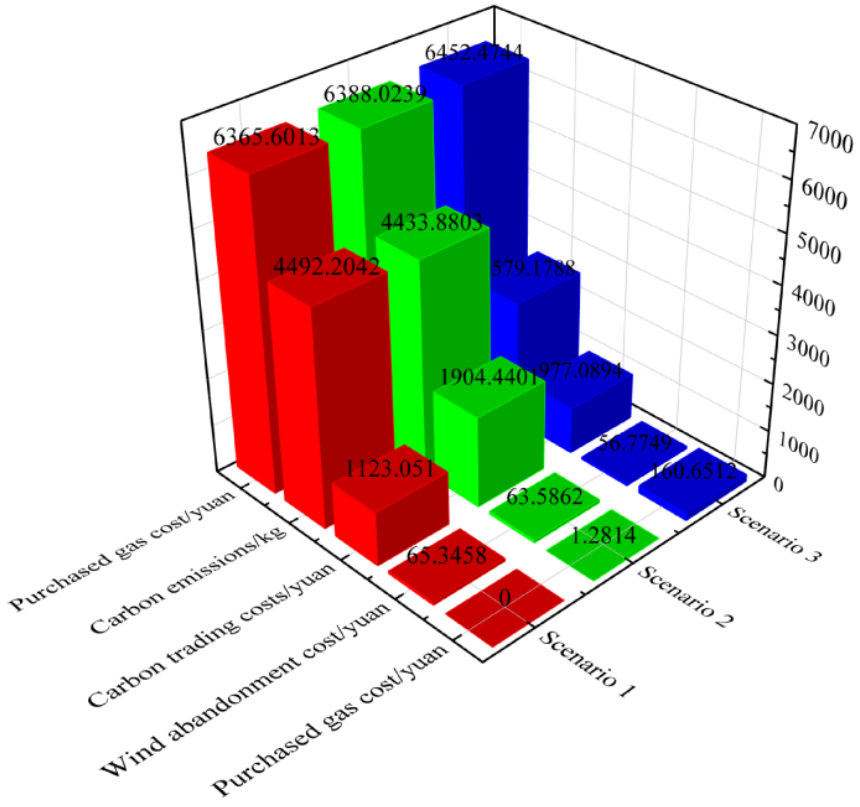

Figure 4. Comparison of Scenarios 1, 2 and 3.

The benefits of ladder carbon trading can be analyzed by comparing Scenario 1 and Scenario 2. From Table 3, it can be seen that Scenario 2 has a higher carbon trading cost of 69.577% compared to Scenario 1 due to the consideration of the ladder carbon trading mechanism, and the average carbon trading price becomes more expensive, which contributes to a decrease in the system's carbon emissions by 58.3 kg. It can also be seen that the total cost of Scenario 2 is higher than that of Scenario 1, which is mainly due to the increase in the cost of carbon trading. From the above analysis, it can be seen that the consideration of the ladder carbon trading mechanism is effective in limiting carbon emissions although it increases the total operating cost of the system, so the next analysis is to consider the introduction of CCS on the basis of the ladder carbon trading to further

reduce the carbon emissions and at the same time to reduce the total operating cost of the system. By comparing Scenario 2 and Scenario 3, it can be seen that Scenario 3, due to the introduction of CCS on the basis of Scenario 2, leads to a decrease in carbon emissions by 1854.7015 kg, with a decrease ratio of 41.83%, and due to the significant decrease in carbon emissions, the cost of carbon trading in Scenario 3 is also greatly reduced, which ultimately leads to a decrease in the total cost of operation of the system by USD 710.3417, with a decrease ratio of 8.5%. It can be noted that the cost of purchased electricity in Scenario 3 is significantly slightly higher than in Scenario 1 and Scenario 2, which is due to the consumption of electricity by the CCS unit. Figure 5 shows the electric power balance of the IES with CCS (the top of the horizontal axis represents the electric energy into the IES, and the bottom of the horizontal axis represents the consumed electric energy, the same as below), in which it can be found that the CCS consumes slightly more electric energy. Table 3 shows that the cost of wind abandonment in all three scenarios is relatively close, indicating that CCS and ladder carbon trading mechanisms have little effect on wind abandonment. After the above analysis, an obvious conclusion can be drawn that the ladder carbon trading mechanism has a certain limiting effect on carbon emissions, but it will make the cost of carbon emissions rise sharply, which will lead to the rise in the total operating costs of the system. However, though the introduction of the CCS can significantly reduce the carbon emissions of the system on the basis of the total operating costs of the system being reduced, so it can be seen that the CCS for the low-carbon economic operation of the system is of a significant size.

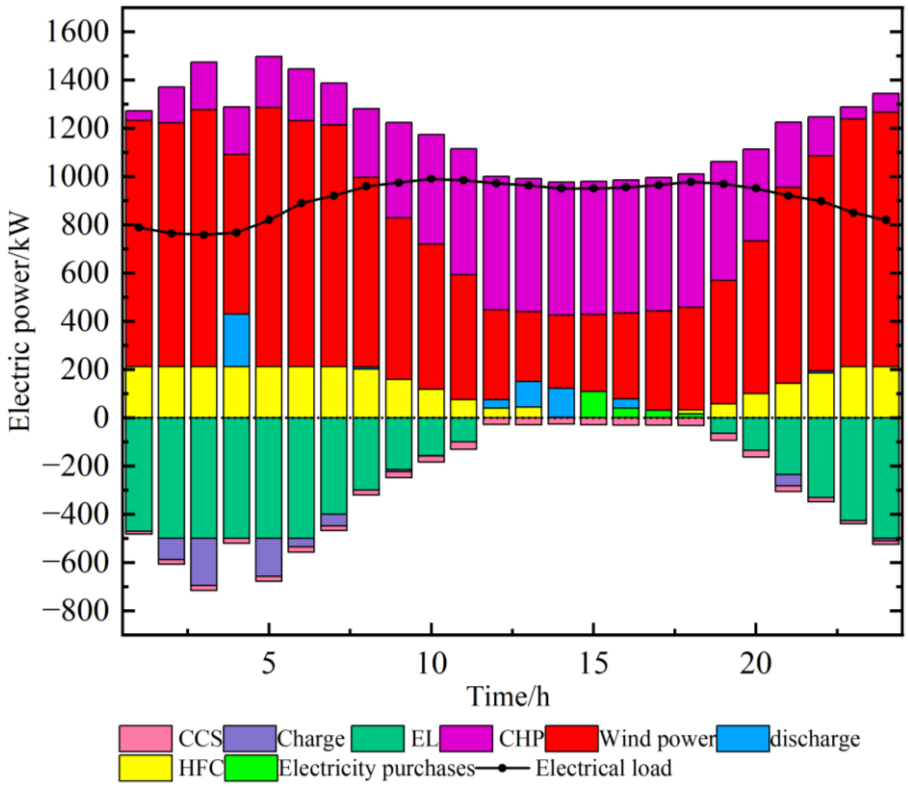

Figure 5. IES electric power balance with CCS.

(2) Impact of the parameters of ladder carbon trading mechanism on the results

The value of the ladder carbon trading mechanism also affects the optimization results of IES, and the optimization results of the system under different values of carbon trading parameters will be analyzed below. Since the core parameter that embodies the ladder carbon trading mechanism is the price growth rate α, and there are few studies in the literature analyzing this parameter, this paper only takes the price growth rate for research and analysis, as shown in Figure 6. Since the value of the price growth rate mainly affects

carbon emissions, carbon transaction costs, and total costs, these three quantities are selected for the study.

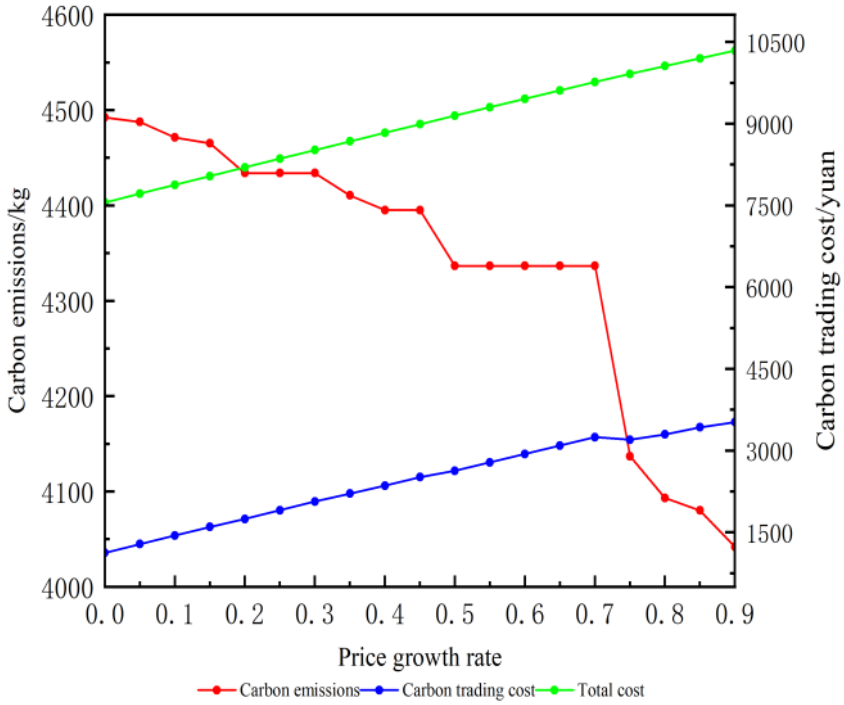

Figure 6. Impact of price growth rates.

As can be seen from Figure 6, when α = [0, 0.45], both the carbon transaction cost and total costs increase with the increase, so in order to reduce the carbon transaction cost, IES will reduce the carbon emissions by adjusting the distribution of the output of the internal equipment. At the same time, due to the inherent load demand within the IES, when $\alpha = (0.45, 0.7]$, the output distribution of the equipment tends to be stabilized, and so does the change in carbon emissions, and it can be observed that the rate of carbon emissions decreases more rapidly after $\alpha > 0.7$. Carbon emissions are reduced by almost 500 kg over the entire $\alpha = [0, 0.9]$ range, which shows that carbon emissions are more sensitive to the comparison.

Combined with the above analysis, the values of different ladder carbon trading mechanisms will affect the optimization results of the system, and the carbon emissions of the system can be accurately guided by the reasonable setting of carbon parameters.

4.2. Analysis of the Benefits of Two-Stage P2G with CCS

In order to study the impact of whether or not to refine the two phases of P2G on the benefits of the system containing CCS, this paper sets up the following two scenarios for comparative analysis.

Scenario 4: The optimized scheduling analysis of integrated energy system with traditional P2G containing CCS.

Scenario 5: The refinement of the optimal scheduling analysis of an integrated energy system with two-phase P2G including CCS.

Figure 7 shows the comparison between scenarios 4 and 5.

The scheduling results for the two scenarios are shown in Table 4, and a comparison shows that:

(1) The carbon emissions of Scenario 5 are reduced by 1094.4029 kg compared to Scenario 4, with a reduction ratio of about 30%. due to the significant reduction in carbon emissions, the carbon transaction cost of Scenario 5 is reduced by USD 547.2015 compared to Scenario 4, with a reduction ratio of about 36%.

(2) The purchased power cost for the Scenario 5 system is approximately USD 119 less than Scenario 4, which is mainly caused by the difference in CCS operation, which will be analyzed later.
(3) The abandonment cost of the Scenario 5 system is significantly lower than that of Scenario 4, with a decrease of 61%, which is mainly due to the difference in the utilization of hydrogen energy in the first phase of P2G, which will also be analyzed.
(4) Scenario 5 outperforms Scenario 4 in all of the above aspects and ends up with lower total system operating costs than Scenario 4.

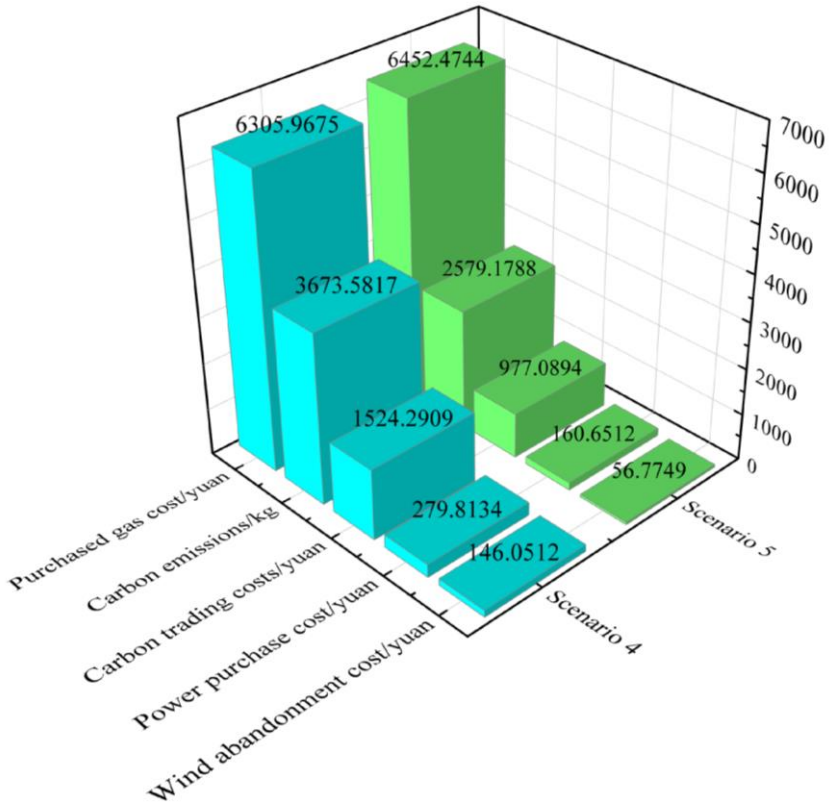

Figure 7. Comparison of Scenarios 4 and 5.

Table 4. Comparison of Scenario 4 and Scenario 5 scheduling results.

Optimization Results	Scenario 4	Scenario 5
Carbon emissions/kg	3673.5817	2579.1788
Carbon trading costs/CNY	1524.2909	977.0894
Power purchase cost/CNY	279.8134	160.6512
Purchased gas cost/CNY	6305.9675	6452.4744
Wind abandonment cost/CNY	146.0512	56.7749
Total cost/CNY	8256.123	7646.9899

The reasons for lower carbon emissions in Scenario 5 than in Scenario 4 are that Scenario 5 builds on Scenario 4 by refining the two phases of P2G, introducing HFC and hydrogen storage equipment to take full advantage of the hydrogen energy generated in the first phase of P2G. For Scenario 4, although the conversion of natural gas by P2G absorbs some CO_2, the combustion of natural gas by the unit releases CO_2 again, and at this time the natural gas combustion of GB and CHP is already in a high carbon emission state, and the CO_2 produced by the combustion of this part of the natural gas will be higher than the absorbed CO_2. For Scenario 5, the hydrogen produced in the P2G stage is directly used for thermoelectricity production via HFC, a process that not only produces no carbon emissions, but also shares a portion of the burden of GB and CHP carbon emissions, so

that Scenario 5 produces lower carbon emissions compared to Scenario 4. Figures 8 and 9 show the IES electrical and thermal power balance diagrams for Scenario 5, respectively. Observing Figure 8, it can be seen that HFC shares part of the electricity production of CHP, and in Figure 9, it can be seen that HFC shares nearly half of the heat production of CHP and GB, and HFC will not produce CO_2 in the process of electricity and heat production, while CHP and GB will release more CO_2 in the process of electricity and heat production, so that the reduction in carbon emissions of the system is precisely from the part of the electricity and heat production that is shared by HFC. That is to say, under the same electrical and thermal loads, the electricity and heat produced by CHP and GB are reduced, and the carbon emissions produced are naturally reduced.

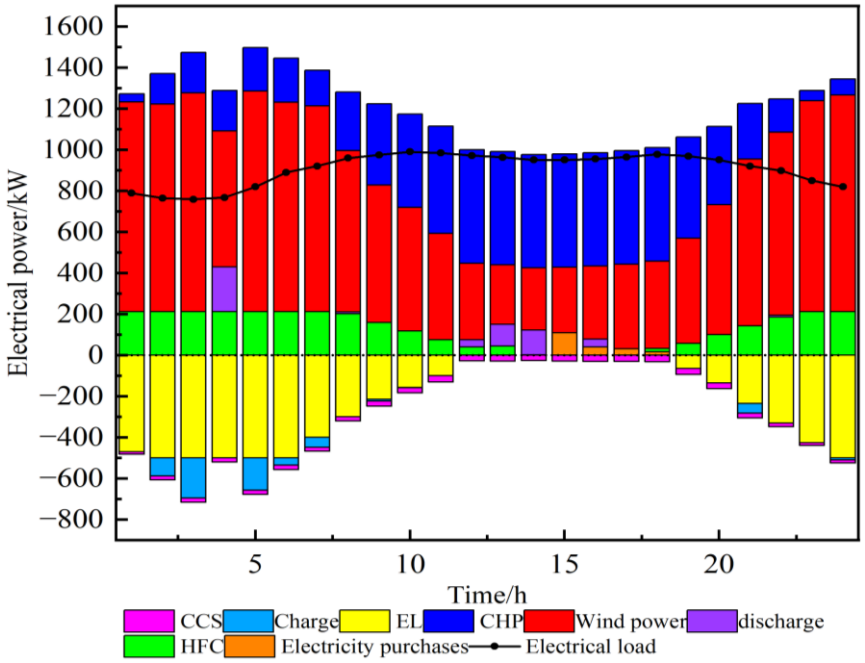

Figure 8. Scenario 5 electric power balance diagram.

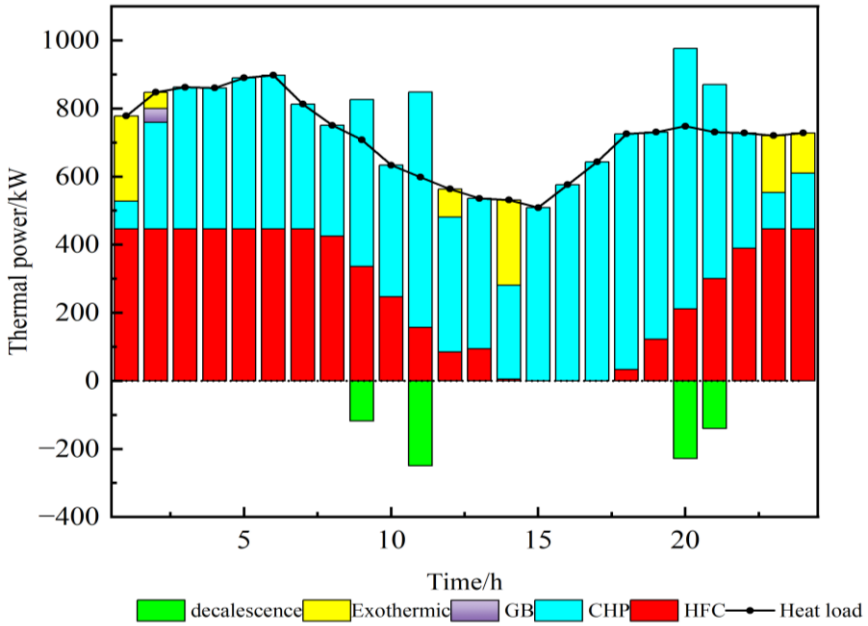

Figure 9. Scenario 5 thermal power balance diagram.

The reasons for the lower cost of purchased electricity in Scenario 5 compared to Scenario 4 are that Scenario 5 refines the two phases of P2G compared to Scenario 4, and the addition of HFC makes full use of the hydrogen produced in the first phase of P2G, sharing part of the electrical and thermal loads, so that the actual outputs of CHP and GB are reduced, which in turn reduces carbon emissions, and makes the power of the CCS reduced compared to that of Scenario 4; therefore the power required by the system is reduced, which in turn lowers the cost of the purchased electricity. Table 5 shows the comparison of the total power consumption and the total purchased power of the system for Scenario 4 and Scenario 5 over the course of a day. As shown in the table, the purchased power in Scenario 4 is 106 kW·h more than that in Scenario 5, while the CCS consumption for Scenario 4 is 135.21 kW·h higher than that in Scenario 5, which is relatively close to each other, indicating that the increase in the purchased power cost is mainly caused by the increase in the CCS consumption. Figure 10 shows a comparison of the magnitude of the CCS operating power for each time period for Scenarios 4 and 5, and it can be seen that the power of the two phases of the CCS operation for each time period of the refined P2G is basically lower than that of the conventional P2G.

Table 5. Scenarios 4 and 5 power purchase and CCS power consumption.

Optimization Results	Scenario 4	Scenario 5	Difference in Value
Purchased electricity (kW·h)	303.5786	196.8765	106.7021
CCS power consumption (kW·h)	702.0275	566.8096	135.2180

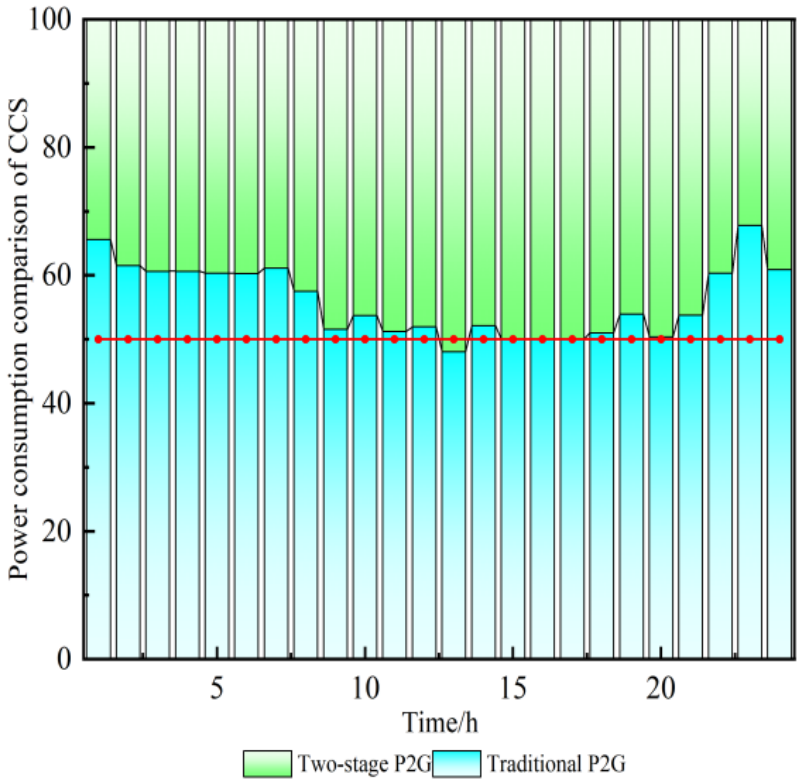

Figure 10. Comparison of Scenario 4 and Scenario 5 CCS Power Consumption.

The reason for the lower abandonment costs in Scenario 5 compared to Scenario 4 are that Scenario 5 incorporates HFC to utilize the hydrogen produced by EL for electricity and heat production compared to Scenario 4. A portion of the excess wind-generated hydrogen can be consumed at night when electricity consumption is low. Part of the H_2 is

stored in hydrogen storage tanks, and part of it is used for HFC power and heat production. Figure 11 shows the hydrogen power balance diagram for Scenario 5, from which it can be seen that the EL is basically operating at full power during the night-time power trough, constantly consuming wind power. Figure 12 shows the wind power output for Scenario 4 and Scenario 5 (Scenario 4 in the left panel and Scenario 5 in the right panel), where the green shaded area is the wind power discarded, and it is clear that Scenario 5 discards much less wind than Scenario 4. In Figure 12, the green shaded area indicates the amount of wind abandonment and the blue shaded area indicates the actual wind power output. The red line above the entire shaded area indicates the predicted wind power output.

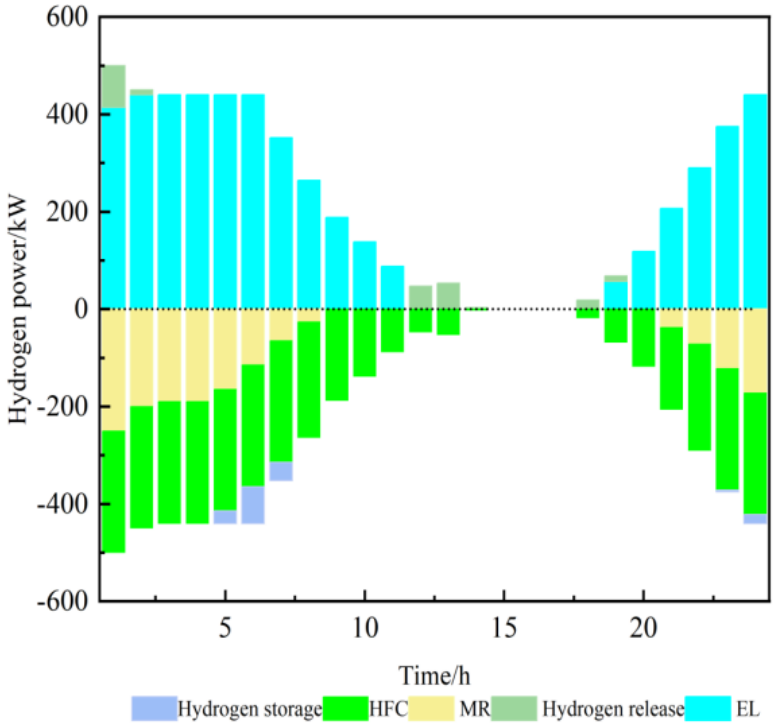

Figure 11. Scenario 5 hydrogen power balance diagram.

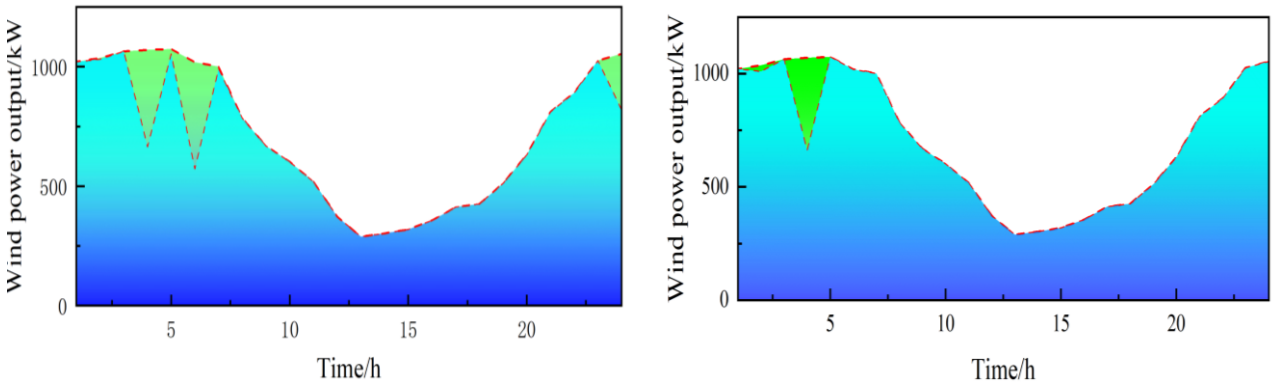

Figure 12. Comparison of wind power abandonment in Scenarios 4 and 5.

4.3. Benefit Analysis Considering CHP and HFC Adjustable Thermoelectric Ratio Characterization

In order to investigate the benefits of CHP and HFC adjustable thermoelectric ratios for the system, the following two scenarios are established for comparative analysis.

Scenario 6: Setting the thermoelectric ratio of CHP and HFC at a constant value (both 1.8).

Scenario 7: Consideration of CHP and HFC thermoelectric ratio adjustable characteristics.

Figure 13 shows a visual comparison of scenarios 6 and 7.

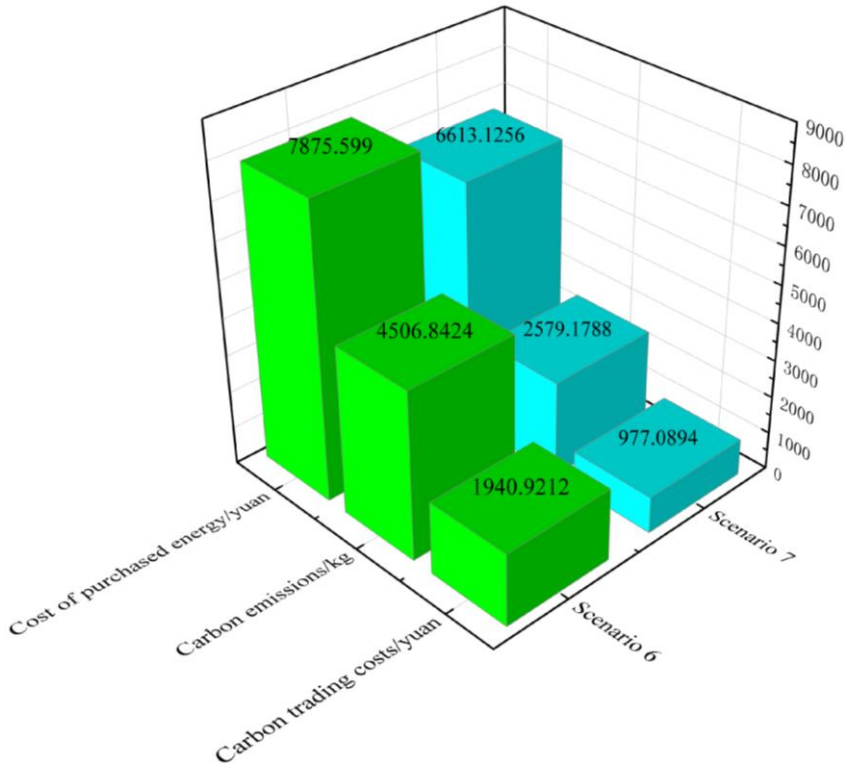

Figure 13. Comparison of Scenarios 6 and 7.

The scheduling results for the above two scenarios are shown in Table 6. As can be seen from the table, after considering the adjustable heat to power ratio, the carbon emissions are reduced by 1927.6636 kg, a ratio of about 42.8%. Carbon trading costs were reduced by USD 963.8318, a rate of about 49.6%. Wind abandonment costs were reduced by CNY 98.0541, a rate of 63.3%. The cost of purchased energy was reduced by CNY 1262.4734, a rate of approximately 16%. The total cost of operating the system was reduced by CNY 2324.3593, a rate of approximately 23.3%. It can be seen that considering the adjustable heat-to-power ratio characteristics of CHP and HFC not only reduces the system's carbon emissions, but also reduces the cost of purchased energy and the cost of wind abandonment, which in turn reduces the total system operating cost.

Table 6. Comparison of Scenarios 6 and 7 scheduling results.

Optimization Results	Scenario 6	Scenario 7
Carbon emissions/kg	4506.8424	2579.1788
Carbon trading cost/CNY	1940.9212	977.0894
Cost of purchased energy/CNY	7875.5990	6613.1256
Total cost/CNY	9971.3492	7646.9899

CHP was analyzed as an example, and Figure 14 shows the 24 h thermoelectric ratio variation in CHP. The figure shows that the thermoelectric ratio of CHP in the night phase has been kept at 2.1, maintaining the maximum value set by this algorithm. Due to the night-phase wind power, output is in the peak period, at the same time the electric load is in the trough period, the wind power has been able to meet the demand of the vast majority of part of the electric load, and at this time at night, the heat load is exactly in the peak period, so in the night phase, in order to improve the efficiency of CHP's energy utilization, its heat and power ratio has been in the maximum state. During the daytime-phase, the electric load is at its peak relative to the thermal load, and considering the effect of time-sharing tariffs, the electricity price is more expensive and the gas price is

cheaper during the daytime, so the CHP will prioritize satisfying the electric load of the system. At this time, the CHP ratio will no longer be maintained at the maximum value, but will be continuously adjusted according to the actual demand of the CHP load and the cost of the system. Since the CHP thermoelectric ratio of Scenario 7 is adjustable, the thermoelectric output can be adjusted in time according to the demand of the load, which improves the efficiency of energy utilization, so it also makes the system respond under the same demand of the load, considering the adjustable characteristics of the thermoelectric ratio will lead to the reduction in the energy that needs to be input into the system, i.e., it reduces the cost of purchasing energy. Combined with the above analysis, it can be seen that Scenario 7, compared with Scenario 6, takes into account the adjustable CHP ratio that is characteristic of CHP, which enables it to adjust its own CHP ratio according to the real-time load demand to achieve the balance of energy supply, and at the same time, reduces the cost of purchasing energy, the cost of operating the system, and the carbon emissions.

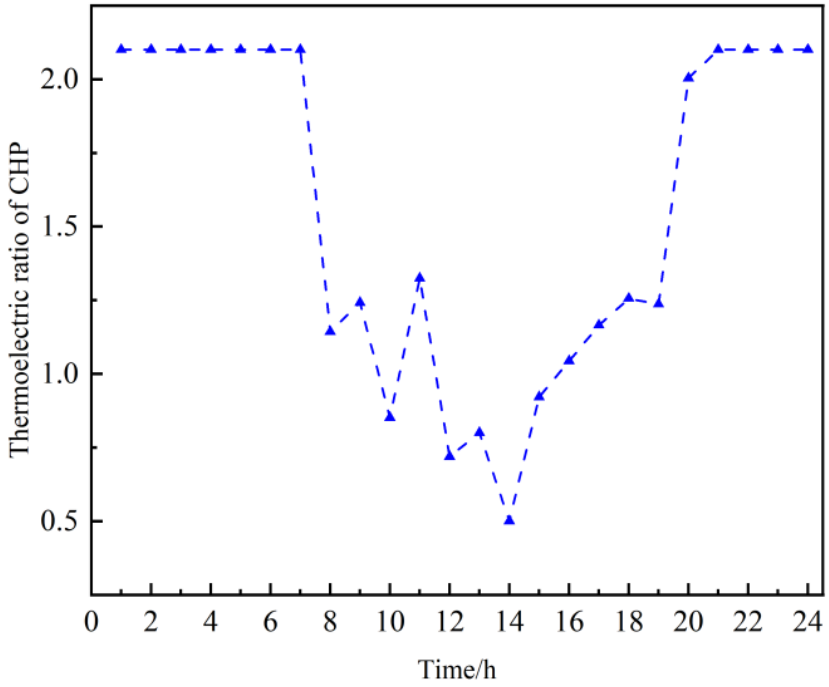

Figure 14. CHP thermoelectric ratio by time period for Scenario 7.

5. Conclusions

In this paper, a two-stage P2G hydrogen-coupled carbon-containing capture (CCS) electricity–heat–hydrogen–gas integrated energy system was established, and the corresponding arithmetic examples were set up to study the benefits brought to the system by the two-stage P2G hydrogen-coupling as well as the adjustable thermoelectric ratio characteristics of CHP and HFC for the CCS and stepped carbon trading mechanism, respectively. In addition, sensitivity analyses of the parameters of the stepped carbon trading mechanism were carried out. The following conclusions were drawn:

(1) The introduction of a laddered carbon trading mechanism will have a limiting effect on carbon emissions, but it will increase the cost of carbon emissions significantly. However, the introduction of CCS can significantly reduce the carbon emissions of the system and at the same time lower the total operating cost of the system. In the context of laddered carbon trading, the introduction of CCS can reduce carbon emissions by 41.83% and system operating costs by 8.5%;

(2) Through the sensitivity analysis of the parameters of the ladder carbon trading mechanism, it is found that the carbon emissions are reduced by nearly 500 kg throughout

the range of α = [0, 0.9], which shows that the carbon emissions are more sensitive to the comparison;

(3) With CCS included, the two-stage P2G hydrogen coupling can further reduce the system's carbon emissions, as well as reduce the system's wind abandonment cost and energy purchase cost, which ultimately leads to a reduction in the total system operating costs. In the CCS-containing case, refining the P2G two-stage and coupling it with HFC and hydrogen storage can lead to a 30% reduction in carbon emissions and a 61% reduction in wind abandonment costs. Carbon trading costs are down by 36% and total system costs are down by about USD 600.

(4) CHP and HFC adjustable thermoelectric bit performance can improve the efficiency of energy utilization, thus reducing the system's carbon emissions, wind abandonment costs and purchased energy costs to a certain extent, thereby reducing the total system operating costs. Considering CHP and HFC adjustable thermoelectric ratios can reduce the cost of purchased energy by 16%, and carbon emissions decreased by 42.7%, carbon trading costs decreased by 49.65%, and total system costs decreased by 23.3%.

Author Contributions: Conceptualization, Z.Z.; Methodology, K.H.; Software, L.Z.; Validation, L.Z.; Formal analysis, Y.G.; Investigation, J.Y.; Data curation, Y.G. and Z.Z.; Writing—original draft, K.H.; Writing—review & editing, K.H.; Supervision, J.Y.; Project administration, K.C. All authors have read and agreed to the published version of the manuscript.

Funding: This work was supported in part by the Changsha Science and Technology Project of Hunan Province under Grant kq2202213, and in part by the National Natural Science Foundation of China's general project under Grant 52177069.

Data Availability Statement: The original contributions presented in the study are included in the article, further inquiries can be directed to the corresponding author.

Conflicts of Interest: The authors declare no conflict of interest.

Appendix A

Table A1. Time-of-day electricity and natural gas tariffs.

Price Type	Time Scale	Value
Electricity price/[CNY (kW·h)$^{-1}$]	01:00–07:00, 23:00–24:00	0.456
	08:00–11:00, 15:00–18:00	0.816
	12:00–14:00, 19:00–22:00	1.44
Gas price/(CNY·m^{-3})	00:00–24:00	0.45

Table A2. Installed capacity and operating parameters of each device.

Installation	Capacity/kW	Energy Conversion Efficiency/%	Climbing Constraint/%
HFC	250	95	20
MR	250	60	20
GB	800	95	20
CHP	600	92	20

Table A3. Installed capacity and parameters of each energy storage.

Installation	Capacity/kW	Lower Capacity Limit/%	Upper Limit Capacity/%	Climbing Constraint/%
Electrical storage	450	10	90	20
Thermal storage	500	10	90	20
Gas storage	150	10	90	20
Hydrogen storage	200	10	90	20

References

1. Zhang, S.; Wang, D.; Cheng, H.; Song, Y.; Yuan, K.; Du, W. Key technologies and challenges of low-carbon integrated energy system planning under dual-carbon target. *Power Syst. Autom.* **2022**, *46*, 189–207.
2. Kang, C.; Chen, Q.; Xia, Q. Research outlook of low-carbon power technology. *Grid Technol.* **2009**, *33*, 1–7.
3. Qiu, D. Path of building green, low-carbon and recycling economic development system in the new era. *J. Soc. Sci. Jiamusi Univ.* **2023**, *41*, 17–19+23.
4. Zhao, X.; Liu, Z.; Li, Y.; Feng, Y.; Lu, Y.; Zhang, J. Research on comprehensive energy planning systembased on "double carbon" target. *Energy Environ. Prot.* **2023**, *45*, 175–178+186. [CrossRef]
5. Cheng, Y.; Zhang, N.; Wang, Y.; Yang, J.; Kang, C.; Xia, Q. Modeling Carbon Emission Flow in Multiple Energy Systems. *IEEE Trans. Smart Grid* **2019**, *10*, 3562–3574. [CrossRef]
6. Secretary of State for Trade and Industry. *Energy White Paper: Our Energy Future-Creating a Low Carbon Economy*; Secretary of State for Trade and Industry: London, UK, 2003.
7. Cheng, Y.; Zhang, N.; Kang, C.; Kirschen, D.; Zhang, B. Research framework and outlookof low-carbon multi-energy systems. *Chin. J. Electr. Eng.* **2017**, *37*, 4060–4069+4285. [CrossRef]
8. Li, K.; Ran, J.; Kim, M.K.; Tian, Z.; Liu, J. Optimizing long-term park-level integrated energy system through multi-stage planning: A study incorporating the ladder-type carbon trading mechanism. *Results Eng.* **2024**, *22*, 102107. [CrossRef]
9. Zou, Y.; Zeng, A.; Hao, S.; Ning, J.; Ni, L. Multi-timescale optimal scheduling of integrated energy system under stepped carbon trading mechanism. *Grid Technol.* **2023**, *47*, 2185–2198. [CrossRef]
10. Guo, R.; Ye, H.; Zhao, Y. Low carbon dispatch of electricity-gas-thermal-storage integrated energy system based on stepped carbon trading. *Energy Rep.* **2022**, *8*, 449–455. [CrossRef]
11. Lei, D.; Zhang, Z.; Wang, Z.; Zhang, L.; Liao, W. Long-term, multi-stage low-carbon planning model of electricity-gas-heat integrated energy system considering ladder-type carbon trading mechanism and CCS. *Energy* **2023**, *280*, 128113. [CrossRef]
12. Luo, Z.; Lai, B.; Bi, G.; Wang, H.; Zhang, T.; Shen, X. Distributed robust optimal scheduling of integrated energy system containing CCUS and P2G. *High Volt. Technol.* **2024**, 1–16. [CrossRef]
13. Chen, J.; Yang, K.; Zhang, Y.; Han, W.; Song, C. Optimized scheduling of integrated energy system under multiple time scales taking into account integrated demand response and carbon capture-electricity-to-gas joint operation. *Power Autom. Equip.* **2024**, *44*, 68–76. [CrossRef]
14. Chen, M.; Lu, H.; Chang, X.; Liao, H. An optimization on an integrated energy system of combined heat and power, carbon capture system and power to gas by considering flexible load. *Energy* **2023**, *273*, 127203. [CrossRef]
15. Zhang, B.; Xia, Y.; Peng, X. Robust optimal dispatch strategy of integrated energy system considering CHP-P2G-CCS. *Glob. Energy Interconnect* **2024**, *7*, 14–24. [CrossRef]
16. Chen, Q.; Wang, J.; Cang, M.; Zhai, X.; Cheng, X.; Wu, S. Optimal scheduling of a township integrated-energy system using the adjustable heat-electricity ratio model. *Glob. Energy Interconnect* **2024**, *7*, 48–60. [CrossRef]
17. Zhang, Y.; Wen, Z.; Wang, C.; Ni, Z.; Yang, S. Optimal scheduling of integrated energy systems considering REGS and adjustable heat-to-power ratio. *Renew. Energy* **2024**, *42*, 241–251. [CrossRef]
18. Chen, J.; Hu, Z.; Chen, Y.; Chen, J.; Chen, W.; Gao, M.; Lin, M.; Du, Y. Thermoelectric optimization of integrated energy system considering stepped carbon trading mechanism and electric hydrogen production. *Power Autom. Equip.* **2021**, *41*, 48–55. [CrossRef]
19. Gao, L.; Fei, F.; Jia, Y.; Wen, P.; Zhao, X.; Shao, H.; Feng, T.; Huo, L. Optimal dispatching of integrated agricultural energy system considering ladder-type carbon trading mechanism and demand response. *Int. J. Electr. Power Energy Syst.* **2024**, *156*, 109693. [CrossRef]
20. Jiang, C.; Ai, X. Research on the operation optimization model of integrated energy system taking into account the uncertainty of multi-energy coupled units. *Grid Technol.* **2019**, *43*, 2843–2854. [CrossRef]